frontiers in Earth Science

ORIGINAL RESEARCH
published: 13 December 2021
doi: 10.3389/feart.2021.760305

A Fossil Paleozoic Subduction-Dominated Trench-Arc-Basin System Revealed by Airborne Magnetic-Gravity Imaging in West Junggar, NW China

*Qifang Zheng, Xi Xu *, Wan Zhang, Yuzhou Zheng, Yinghui Liu, Xingtao Kuang, Daoqing Zhou, Xuezhong Yu and Baodi Wang*

China Aero Geophysical Survey and Remote Center for Natural Resources, China Geological Survey, Beijing, China

A Carboniferous trench-arc-basin system related to oceanic slab subduction has been thoroughly imaged by various geophysical probing approaches and proposed for the formation of West Junggar, Northwest China, located in the southwest of the Central Asian Orogenic Belt. However, debate on the origin of West Junggar still continues. Here, we present an integrated aeronautic magnetic–gravity observation to further identify the trench-arc-basin system and constrain the subduction mode. By deploying an integrated aerial magnetic–gravity survey consisting of 66,000 survey-line kilometers from August 3, 2015 to April 22, 2016, we determine the magnetic and gravitational anomaly across the study region by using geophysical potential-field processing. Our results reveal curial crust-scale variations in magnetic and gravitational structures beneath West Junggar and that a prominent Bouguer gravity high is located between the Darbut and Karamay–Urho faults, likely corresponding to a trapped oceanic slab. Notably, the Tacheng Basin is characterized by high-frequency magnetic signal and gravity highs, as well as the Carboniferous rifting–related sedimentary cover, which could be reasonably interpreted to be a back-arc basin. Integrated with these comprehensive geological and geophysical observations across West Junggar, the previous model of West Junggar trench-arc-basin system related to a fossil intra-oceanic subduction during the Late Paleozoic is further renewed.

Keywords: West Junggar basin, subduction-dominated trench-arc-basin system, geophysical potential field processing, magnetic and gravity structure, Late Paleozoic, Tacheng Basin

OPEN ACCESS

Edited by:
Lei Wu,
Zhejiang University, China

Reviewed by:
Jinchang Zhang,
South China Sea Institute of Oceanology (CAS), China
Jien Zhang,
Institute of Geology and Geophysics (CAS), China

****Correspondence:***
Xi Xu
winbreak@163.com
lexus.phd@gmail.com

Specialty section:
This article was submitted to Structural Geology and Tectonics, a section of the journal Frontiers in Earth Science

Received: *18 August 2021*
Accepted: *26 October 2021*
Published: *13 December 2021*

Citation:
Zheng Q, Xu X, Zhang W, Zheng Y, Liu Y, Kuang X, Zhou D, Yu X and Wang B (2021) A Fossil Paleozoic Subduction-Dominated Trench-Arc-Basin System Revealed by Airborne Magnetic-Gravity Imaging in West Junggar, NW China. Front. Earth Sci. 9:760305. doi: 10.3389/feart.2021.760305

INTRODUCTION

As the largest Phanerozoic accretionary domain in the world, the Central Asian Orogenic Belt (CAOB), also termed as the Altaid tectonic collage, is a wide orogenic collage during the Paleozoic closure of the Paleo-Asian Ocean, and the amalgamation of diverse-origin terrains, including island arcs, seamounts, accretionary wedges, oceanic plateaus, and, possibly, micro-continents (Jahn et al., 2000; Kröner et al., 2007, 2008; Sengör et al., 1993; Windley et al., 2007; Xiao et al., 2015; Wu et al., 2018; Zhang et al., 2021; **Figure 1**).

Situated in the southwestern CAOB, the West Junggar is bounded by the Junggar Basin to the east, the Kazakhstan Shield to the west, the Altaid Orogen to the north, and the Tian Shan Orogen to the south (Buckman and Aitchison, 2004; Coleman, 1989; Feng et al., 1989; **Figure 1**) and is mainly considered as an accretionary collage formed by subduction and accretion processes during the Neoproterozoic and Late Paleozoic (Feng et al., 1989; Windley et al., 2007; Xiao et al., 2009; Zhang et al., 2011a; Zhang et al., 2018, 2021) and characterized by the Paleozoic ophiolites, magmatic rocks, and numerous valuable Cu-Au–bearing ore deposits distributed along the NE-oriented Hatu, Karamay–Urho, and Darbut faults (Chen and Arakawa, 2005; Xu et al., 2006; He et al., 2007). As an ideal natural laboratory to decipher the tectonic evolution of the CAOB, though several widely-accepted competing models have been built based on multidisciplinary geological, geochemical, and geophysical data, there is still controversy on the intra-oceanic arc system with a ridge-trench interaction generated in double subduction zones (Zhang et al., 2011a; Zhang et al., 2011b; Ma et al., 2012; Yang et al., 2013), a single subduction zone (Su et al., 2006; Xiao et al., 2008; Xu et al., 2016, 2020), or an intra-continental zone (Zhang and Huang, 1992; Chen and Arakawa, 2005; Geng et al., 2009). These different subduction models would correspond to different crustal structures recorded during the subduction process (Xu et al., 2016; Xu et al., 2020; Wu et al., 2018). Thus, imaging the high-resolution crustal structure helps discriminate among the competing models.

Over the past five years, there have been a number of geophysical studies conducted across the West Junggar, such as MT (Xu et al., 2016; Xu et al., 2020; Zhang et al., 2017; Liu et al., 2019) and seismic sections (Wu et al., 2018). These studies together reveal detailed crust structures beneath the domain, mostly by 2D profiling (e.g., Xu et al., 2016) or 3D inversion (Xu et al., 2020). However, other types of geophysical methods lag behind, especially the aeronautic magnetic and gravimetric survey, which could provide regional continental-scale coverage and extra constraints on physical properties such as magnetization and density, respectively, although some recent efforts in detecting electrical structures of the crust and upper mantle of West Junggar have been taken. This imbalance in utilizing different geophysical techniques hinders thoroughly integrating all available geophysical data and systematically deciphering all key regional tectonic units in the area. Our purpose of this study is to characterize comprehensively the geology and geophysics of the West Junggar domain with an integrated approach, and then draw conclusions from our new data processing and interpretation schemes by using a large set of newly-acquired gravimetric and magnetic data.

REGIONAL GEOLOGICAL AND GEOPHYSICAL SETTING

Geological Setting

West Junggar is bounded by the Tian Shan Orogenic Belt in the south, the Altaid Orogenic Belt in the north, the Junggar Basin in the east, and the Kazakhstan Block in the west. It experienced a long-term history of Paleozoic accretion (Yang et al., 2012).

The West Junggar is depicted by a series of island arcs and accretion complexes, partitioned by the Darbut, Barleik, and other faults, oriented in the NE–SW regions (Li et al., 2014). The Carboniferous and Devonian sandstone and volcanic rocks including andesite, andesitic basalt, and basalt are dominantly prevalent in these complexes (Yang et al., 2015a; Zhang et al., 2011a; Zhang et al., 2011b; Zhang et al., 2018; Zhang et al., 2021; Han et al., 2018). The granitoids are classified as the A-type and the I-type. The granitoids, adakites, and charnockites in this region could be dated back mostly between the Middle–Late Carboniferous and Permian eras (e.g., Yang et al., 2015b; Zhang et al., 2021). There are two well-exposed NE–SW–trending Darbut and Karamay ophiolitic mélanges, which are the most striking geological features across the West Junggar (Chen et al., 2014; Zhang et al., 2018). Extending more than 200 km, the northeast-striking Darbut fault is known as a Permian and younger high-angle strike-slip fault across the West Junggar region (Allen et al., 1995; Zhang et al., 2018; Xu et al., 2016). Distributed regionally over a distance of 100 km, these continuous stratigraphic sections on both sides of the Darbut fault have been divided into the Tailegula, Baogutu, and Xibeikulasi formations from the bottom to the top (Chen et al., 2014; Zhang et al., 2018, 2021). In the Tacheng Basin, the sedimentary strata were filled with the Late Paleozoic and Cenozoic strata. However, its basement is unknown (Li et al., 2015a,b). The ophiolitic mélanges and the sedimentary series between the Dagun and the Baijiantan were interpreted as Carboniferous accretionary complexes (Zhang et al., 2011a; Choulet et al., 2012). Zhang et al. (2011a) supposed there are two accretionary complexes that are generated in two subduction zones, whereas Choulet et al. (2012) suggested a single subduction complex.

2.2 Regional Physical Properties

In terms of the susceptibility statistics and geological background of the West Junggar region, the magnetic feature for the sedimentary strata can be expressed by a simple physically magnetic model. As shown in **Table 1**, all sedimentary strata have either no or weak magnetization (with susceptibility less than 100×10^{-5} SI). Only the sedimentary strata inlaid with magma-related rock present some weak or medium magnetization (greater than 100×10^{-5} SI but less than 500×10^{-5} SI). In contrast, the Devonian and Carboniferous magmatic rocks, being composed of more mafic components, have extremely greater susceptibility values, varying from 116×10^{-5} to $11{,}024 \times 10^{-5}$ SI, with an arithmetic mean of about $2{,}280 \times 10^{-5}$ SI (**Table 1**). These high-susceptibility rocks are inferred to be the main contributor to the variation of local magnetic anomalies. Furthermore, the Carboniferous and Permian intrusive rocks varying from acidic to basic–ultrabasic are magnetically measured (**Table 2**). The mafic intrusive rocks have very strong susceptibility, while the acidic rocks are relatively weak susceptibility. It is notable that the Junggar Precambrian crystalline basement, consisting of highly metamorphic or mafic rocks and underlying the sedimentary

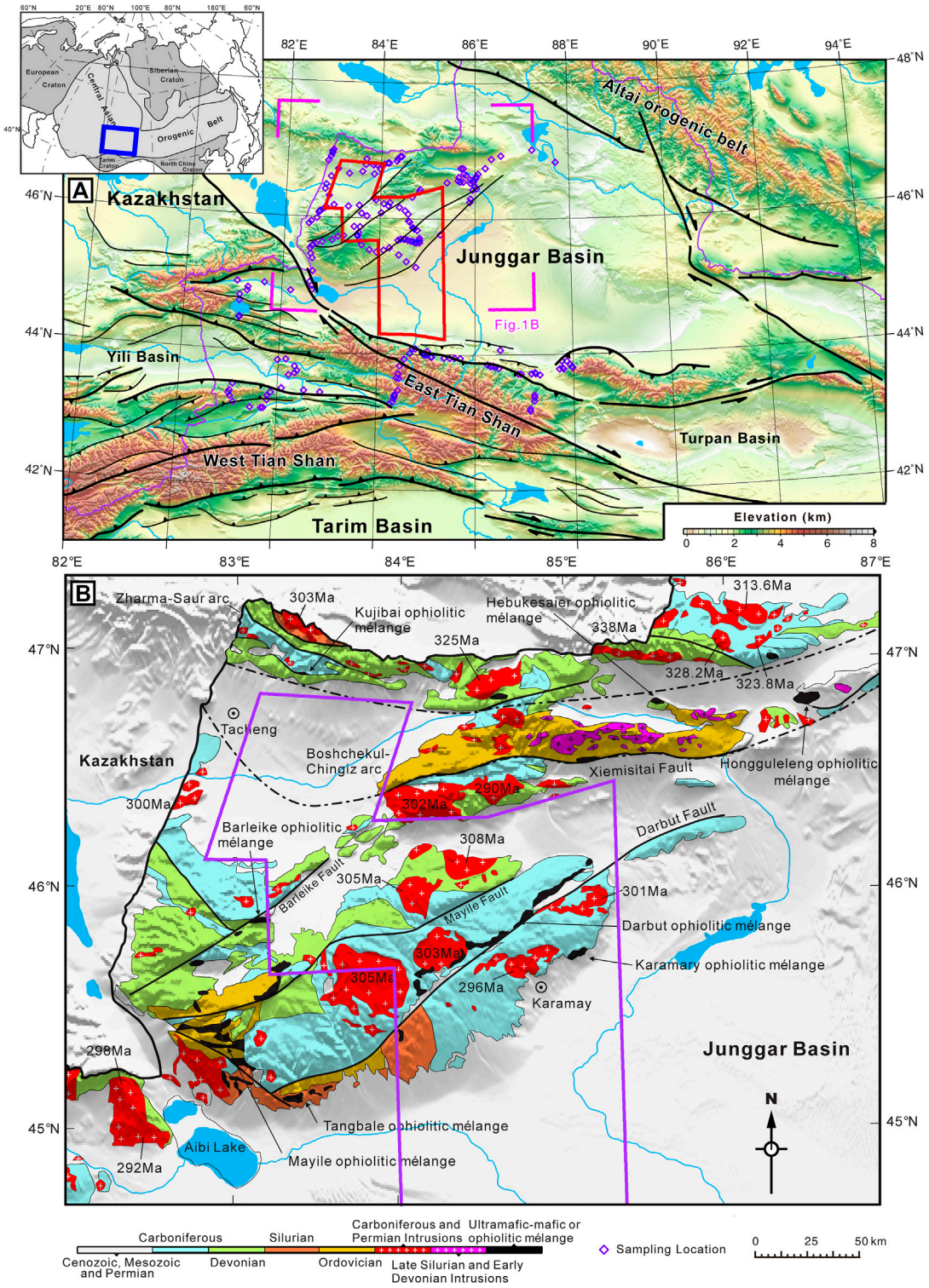

FIGURE 1 | (A) Topography of the Junggar Basin and its environs in northwestern Xinjiang Province. The red polygon is the region of aerial magnetic and gravity data acquired in this study. The blue-pink rhombus indicates the locations for measuring the magnetic susceptibility and density of sampling rocks. The measured magnetic susceptibility and density data are compiled in **Table 1** and **Table 2**. The tectonic framework is modified from Jahn et al. (2004) and Windley et al. (2007). **(B)** Simplified geological map of the West Junggar Basin and its adjacent tectonic units [XJBGMR (Bureau of Geology and Mineral Resources of Xinjiang Province), 1993; Li et al., 2014].

TABLE 1 | Measured physical properties of exposure strata in the West Junggar.

Era	Lithology	Density (g/cm^3)				Magnetic susceptibility (×10^{-5} SI)			
		Number	Min	Max	Mean	Number	Min	Max	Mean
Q	Gravel soils					32	17	300	112
N	Sandstone					2	2	85	26
E									
K									
J	Sandstone, conglomerate	7	2.22	2.59	2.42	8	2	323	52
T									
P	Limestone	1	2.79	2.87	2.87	1	44	100	71
	Sandstone	1	2.60	2.62	2.61	1	4	59	22
	Tuff breccia	1	2.55	2.58	2.56	1	89	405	209
C	Sandstone, mudstone	5	2.52	2.70	2.65	7	8	98	37
	Limestone	4	2.69	2.92	2.76	5	6	510	24
	Acidic volcanic (clastic) rock and tuff	8	2.55	2.75	2.63	8	4	1827	257
	Intermediate basic (sub)volcanic rock	5	2.64	2.83	2.74	6	116	11,024	2,286
	Mafic rock	1	2.76	2.92	2.83	1	6	5,596	2,559
D	Mudstone, sandstone, silty sandstone, and conglomerate	13	2.53	2.74	2.62	18	2	245	50
	Limestone	4	2.67	2.81	2.74	4	0	123	34
	Tuff, pyroclastic rock, felsite	7	2.55	2.83	2.64	9	4	2,710	446
	Intermediate-basic volcanic rock, sub-volcanic rock	2	2.67	2.73	2.71	2	1,108	3,789	2,236
S	Sandstone	1	2.65	2.68	2.67	1	17	46	31
	Limestone	2	2.68	2.74	2.72	2	14	99	49
	Pyroclastic rock	1	2.75	2.80	2.77	1	91	572	227
O	Limestone	1	2.99	3.04	3.01	1	55	105	80

**Number in the column of density and magnetic susceptibility indicates the count of measured locations. In each location, there could be a series of measuring points or samples.*

cover, also possesses extremely strong susceptibility, which is the origin of regional long-wavelength magnetic anomalies across the Junggar Basin. Although these basement-related rocks are not directly measured in our field work, there are a lot of detailed data published in previous literature (Xiong et al., 2016).

In the rock density statistics (**Tables 1**, **2**), various density types are presented. In order to compare each density type in an effective way, the average density is taken as the reference data. The density of sandstone and its derivants vary from 2.49 g/cm^3 to 2.65 g/cm^3, while limestone presents high density values distributed between 2.76 and 3.01 g/cm^3. The magmatic rocks of various types show intermediate density values with a variation range from 2.63 g/cm^3 to 2.83 g/cm^3. Generally, sandstone is mainly derived from terrestrial geologic settings, while limestone is directly related to marine geological settings (Tong et al., 2018). Moreover, the magmatic rocks are all originated from the reworking of the crust–mantle interaction (Tong et al., 2018). Hence, the obvious density contrast could be used to indicate the change in structural and tectonic settings.

DATA AND METHOD

Aerial Magnetic and Gravity Data Measurement

The integrated aeronautic magnetic–gravity measurement across the West Junggar was conducted by Group 913 of the Geophysical Prospecting Department, China Aero Geophysical Survey and Remote Sensing Center for Natural Resources (AGRS), China Geological Survey, and funded with more than 1.4 million dollars from the Geological Survey Project of Comprehensive Airborne Gravity and Magnetic Survey in the Western Junggar Basin. The aerial magnetic and gravity data were measured by using the helium optical pumping magnetometer and the Russian GT-1A airborne gravity meter system, respectively. The magnetic and gravity measurement instruments were integrated in a Cessna 208 aircraft platform with ID number B-9820, permitted by the Zhuhai AVIC General Aviation Co., Ltd., from August 3, 2015 to April 22, 2016. In total, 66,000 km of survey lines were required by 99 sorties, including 62,700 km of the measuring lines and 3,300 km of the crossing lines (**Figure 2**). The survey scale is 1:50,000 with 500-m measuring and 10,000-m crossing flight-line spacing, and the flight altitude ranges from 1,100 to 2,300 m (**Figure 2**).

The total-filed aeromagnetic data and free-air airborne gravity data were finally acquired by preprocessing field data. The field-measured magnetic–gravity data of each sortie were timely preprocessed. The airborne gravity data were processed by the software packages of Gravimetric Technologies (Russia) and OASIS Montaj. The original aeromagnetic data were processed by the aeronautical geophysical data processing system (AGRS-GeoProbe, http://www.agrs.cn/cgzt/xxcp/448.htm). Compared with the public magnetic dataset (EMAG2; http://www.geomag.org/models/emag2.html) and free-air gravity database (Sandwell et al., 2013; Sandwell et al., 2014), the aerial magnetic and gravity data could present more details (**Figures 3**, **5**). Compared to the public magnetic data (**Figure 3A**), a series of high-amplitude, long-wavelength magnetic anomalies have been overlaid by several short-wavelength, positive linear anomalies (**Figure 5A**) across the northern and eastern portions of West Junggar.

Figure 5B illustrates the regional map of anomalies in airborne Bouguer gravity. As anticipated, such anomalies are positively associated with topography. Hence, the southwest region of Karamay's elevated topography (**Figure 5B**)

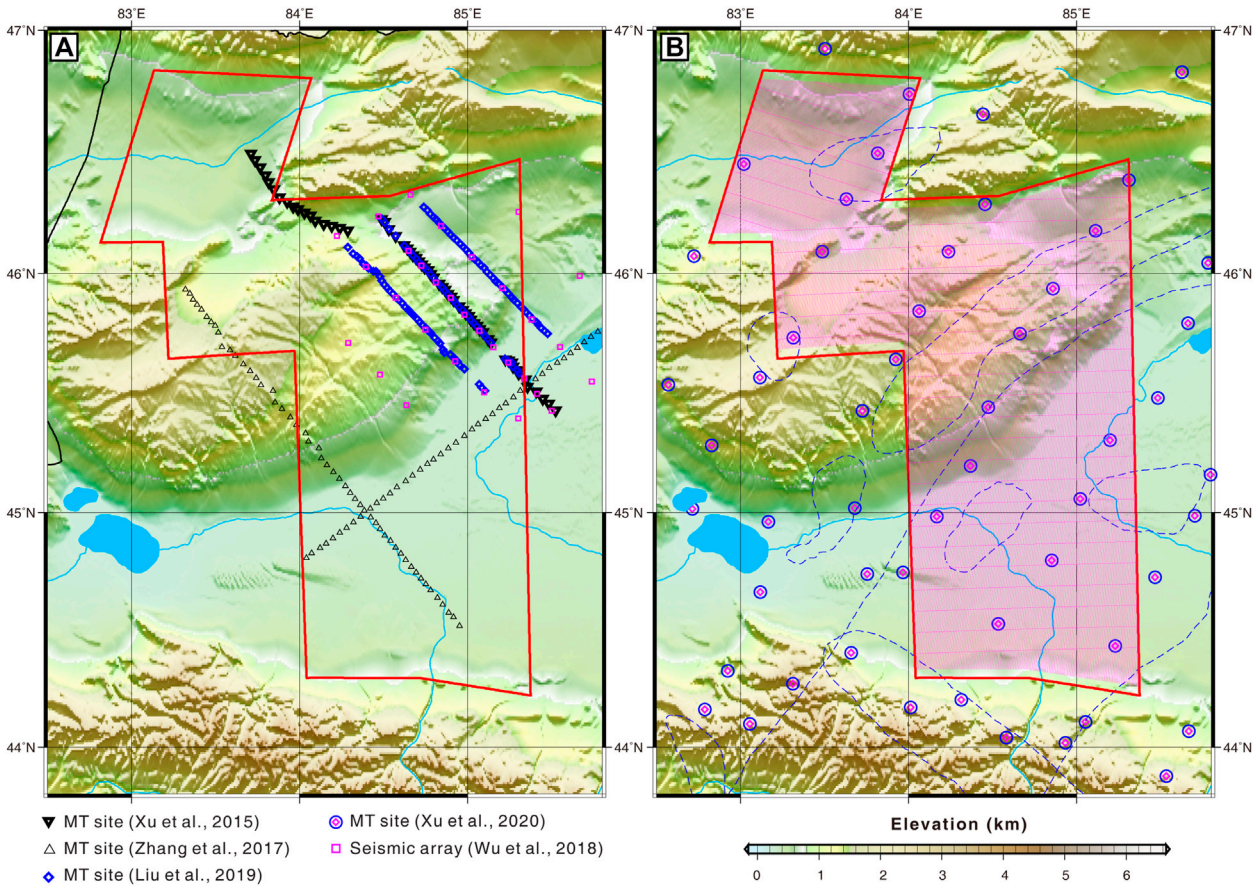

FIGURE 2 | Previous geophysical probe **(A)** and airborne magnetic–gravity probe **(B)** across the West Junggar. The thick-line black triangles, thin-line black reversal triangles, blue rhombus, and blue circle-enclosed pink rhombus indicate the magnetotelluric (MT) sites of Zhang et al. (2017); Xu et al., (2015); Liu et al. (2019); and Xu et al. (2020), respectively. The pink squares are seismic arrays (Wu et al., 2018). The red polygon is the region of aerial magnetic and gravity data acquired in this study. The pink lines in the red polygon are the survey lines. The blue dotted line curves are the boundaries of the lithosphere-scale lower resistivity anomalies (Xu et al., 2020). Overlapped on the maps are major rivers and lakes.

TABLE 2 | Measured physical properties of exposure strata across the West Junggar.

Lithology	Era	Density (g/cm^3)				Magnetic susceptibility (×10^{-5} SI)			
		Number	Min	Max	Mean	Number	Min	Max	Mean
Acidic intrusive rock	Granite (C/P)	7	2.58	2.69	2.62	9	28	2,500	483
	K-feldspar granite (C/P)	4	2.51	2.63	2.58	5	20	685	180
	Monzonitic granite	1	2.51	2.58	2.56	1	38	269	142
Intermediate-acid intrusive rock	Granodiorite (C)	1	2.75	2.76	2.76	1	19	76	46
Basic–ultrabasic intrusive rock	Gabbro, ultrabasic rock	2	2.73	2.89	2.82	2	213	6,215	2,587

**Number in the column of density and magnetic susceptibility indicates the count of measured locations. In each location, there could be a series of measuring points or samples.*

manifests high gravity values suggesting the basement high along Karamay. The southern portion of the study area signifies a relatively shallow basement which is gravity low.

As the key parameters in the identification of geophysical features, the magnetic susceptibility and density of the sedimentary strata and magmatic rock are the curial constrains on the geological interpretation of magnetic and gravitational anomalies across the West Junggar region. In the field, we measured *in situ* the magnetic susceptibility data for different strata and magmatic rocks in more than 128 exposed locations across the West Junggar and its surrounding regions and measured indoor density data for these related rock and strata samples, totally

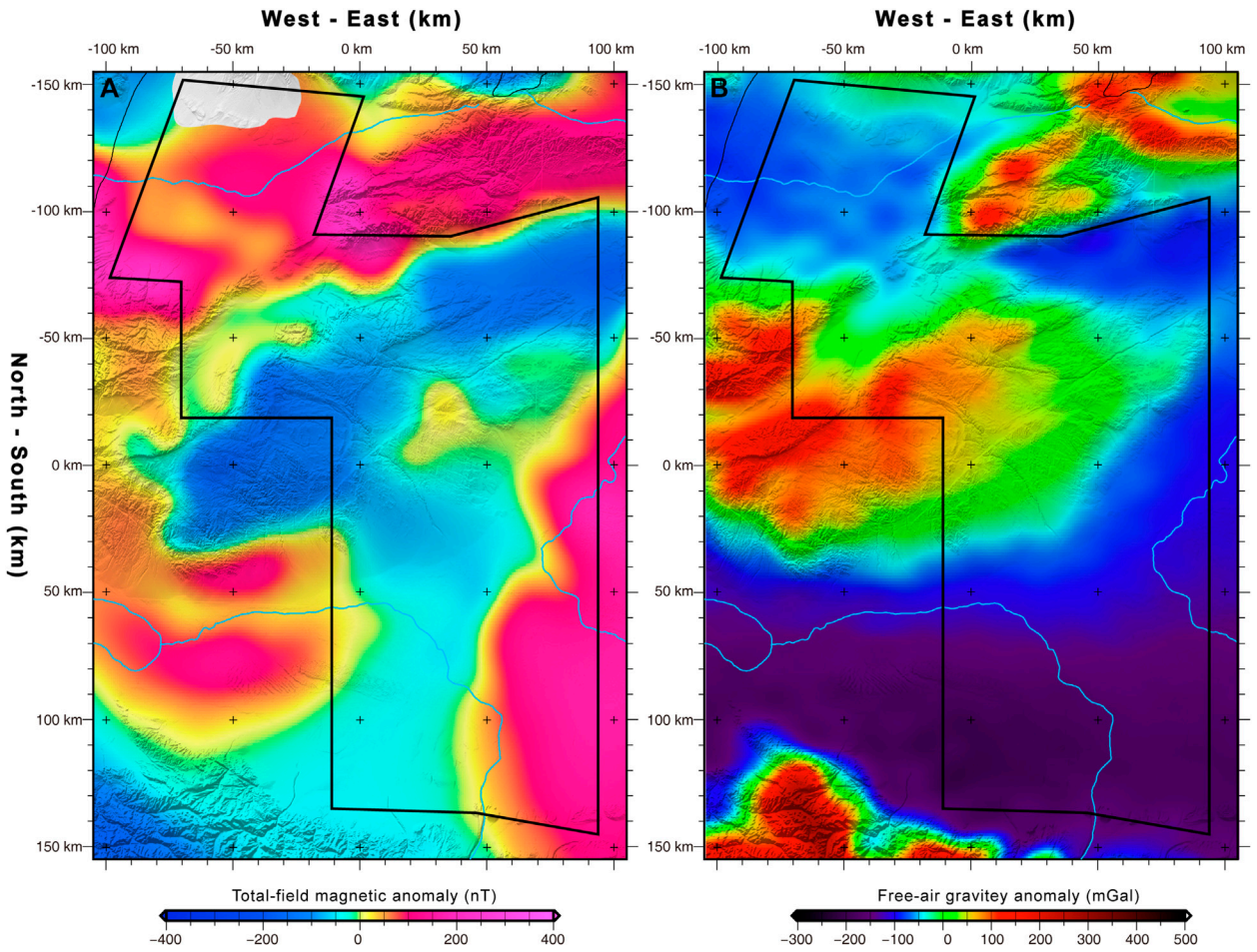

FIGURE 3 | (A) Map of total-field magnetic anomalies derived from the EMAG2 dataset (http://www.geomag.org/models/emag2.html). **(B)** Map of free-air gravity anomalies derived from Sandwell et al. (2013 and 2014). Both maps are overlain on the shaded ETOPO model (www.ngdc.noaa.gov/mgg/global.html).

79. Detailed petrophysical property statistics of susceptibility and density in this study are collated and compiled in **Table 1**, **2**.

Aerial Magnetic and Gravity Data Processing

Reduction to the Pole and Analytical Signal Amplitude for Magnetic Data

To eliminate the effect of oblique magnetization, the reduction to the pole (RTP) of the magnetic anomaly is a primary processing technique. The RTP-corrected magnetic data can accurately promote data interpretation and relocate magnetic boundaries. Subsequently, we applied the RTP method of variable inclination (Arkani-Hamed, 1988) to process the aeromagnetic data.

In order to enhance the magmatism-derived signal, the processing of analytical signal amplitude could effectively quantify the magnitude and location of subduction-related magmatism as follows:.

$$A(x, y) = (\partial M/\partial x)\vec{x} + (\partial M/\partial y)\vec{y} + i(\partial M/\partial z)\vec{z}, \quad (1)$$

where $\vec{x}$, $\vec{y}$, and $\vec{z}$ unit vectors are in x, y, and z directions, respectively, and M is the magnetic field anomaly (Nabighian, 1984; Ofoegbu and Mohan, 1990; Roest et al., 1992).

According to Roest et al. (1992), the analytic signal amplitude (ASA) is obtained through the vector addition of the imaginary component in the vertical direction and the two real components in the horizontal direction. Assuming vertical contact models, it is independent of inclinations and declinations of source magnetizations (Agarwal and Shaw, 1996; Salem et al., 2002; Li, 2006). As being dependent only on first-order derivatives, the ASA is easy to calculate and actually equivalent to the total magnetic gradient as follows:

$$A(x, y) = \sqrt{(\partial M/\partial x)^2 + (\partial M/\partial y)^2 + (\partial M \mid \partial z)^2}. \quad (2)$$

The RTP-corrected and ASA-processed algorithms are integrated in the AGRS-Geoprobe software package (http://www.agrs.cn/cgzt/xxcp/448.htm), developed by AGRS, China Geological Survey. We processed the aeromagnetic data on the AGRS-Geoprobe software platform and plotted the aeromagnetic

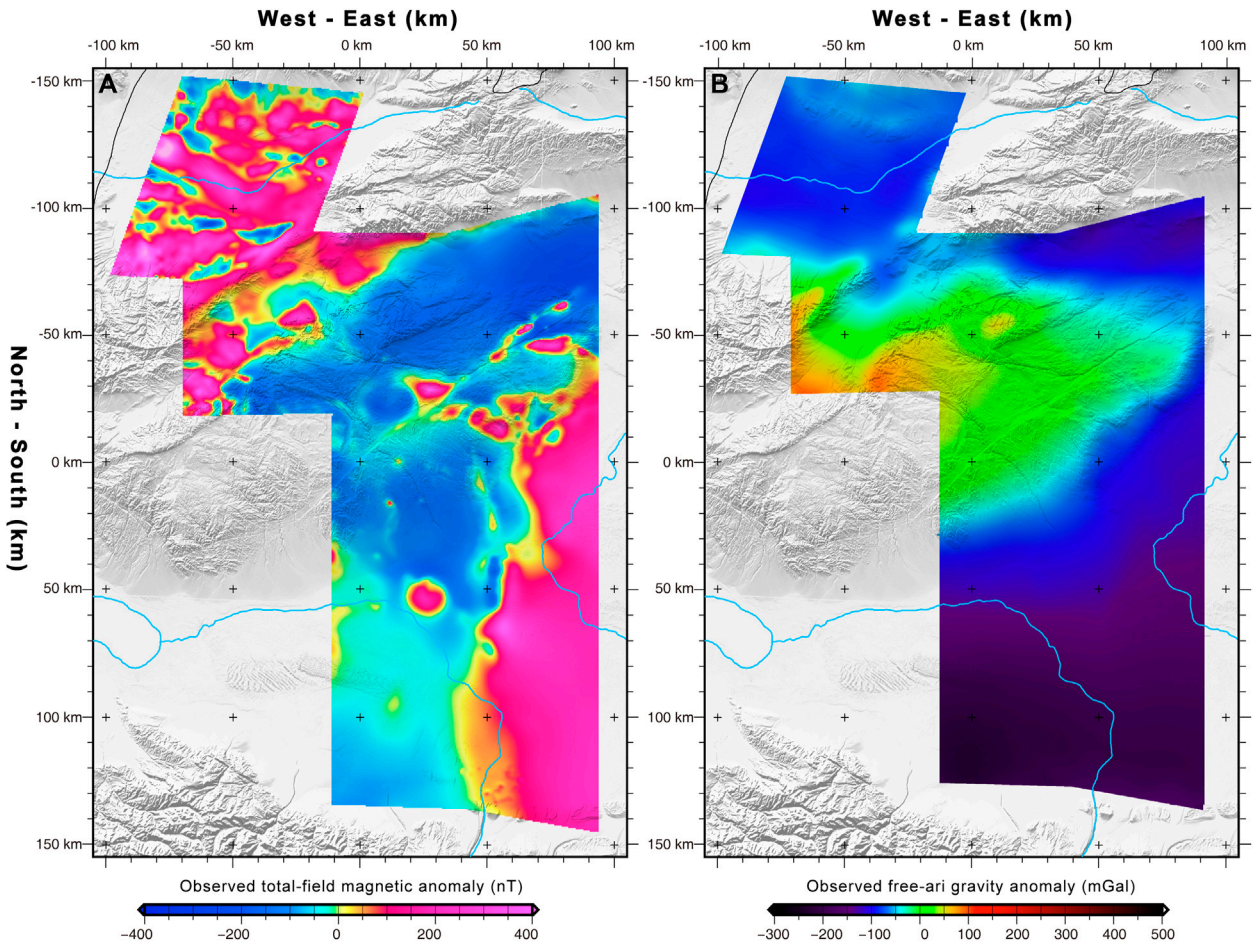

FIGURE 4 | (A) Map of observed total-field magnetic anomalies in this study. The warm red and cool blue colors depict magnetic highs and lows, respectively. **(B)** Map of observed free-air gravity anomalies in this study. Both maps are overlain on the shaded ETOPO model (www.ngdc.noaa.gov/mgg/global.html).

maps using the Generic Mapping Tools (GMT) software package (Wessel et al., 2013).

Bouguer Correction for Gravity Data

The Bouguer gravity data were obtained from observed free-air gravity data by removing the effects of the topography. We used GT-1A Gravity software of aerial gravity data processing, integrated on the Oasis Montaj of Geosoft, to preprocess the field gravity data acquired by the GT-1A airborne gravimetry measurement system. It is notable that GT-1A Gravity software was co-developed by the Navigation and Control Laboratory of Lomonosov, Moscow State University and Gravimetric Technologies, Russia. The primitive aerial gravity data measured in the field were successively processed by the GTNav, GTQC20, and GTGrav modules in the GT-1A software package and then transformed to be the original free-air airborne gravity data. Furthermore, data were processed in turn by coordinate projection conversion, data editing, data leveling, and data–noise processing on the Oasis-based AirGrav module. Followingly, terrain correction and Bouguer anomaly calculation were carried out within the relevant module units. Finally, the airborne Bouguer gravity anomaly data were produced. In the terrain correction, the topographic data were derived from the ETOPO model (www.ngdc.noaa.gov/mgg/global.html) and corrected by the geoidal surface of Yellow Sea 1956 height.

RESULT

Figure 5A reveals that RTP correction of aeromagnetic anomaly is a necessary step to accurately define tectonic units and outline their magnetic boundaries, varying from −281.3 nT to + 994.2 nT, with remarkable contrast between regional and local magnetic anomalies. Especially, the regional fault (such as the Darbut fault) is better characterized

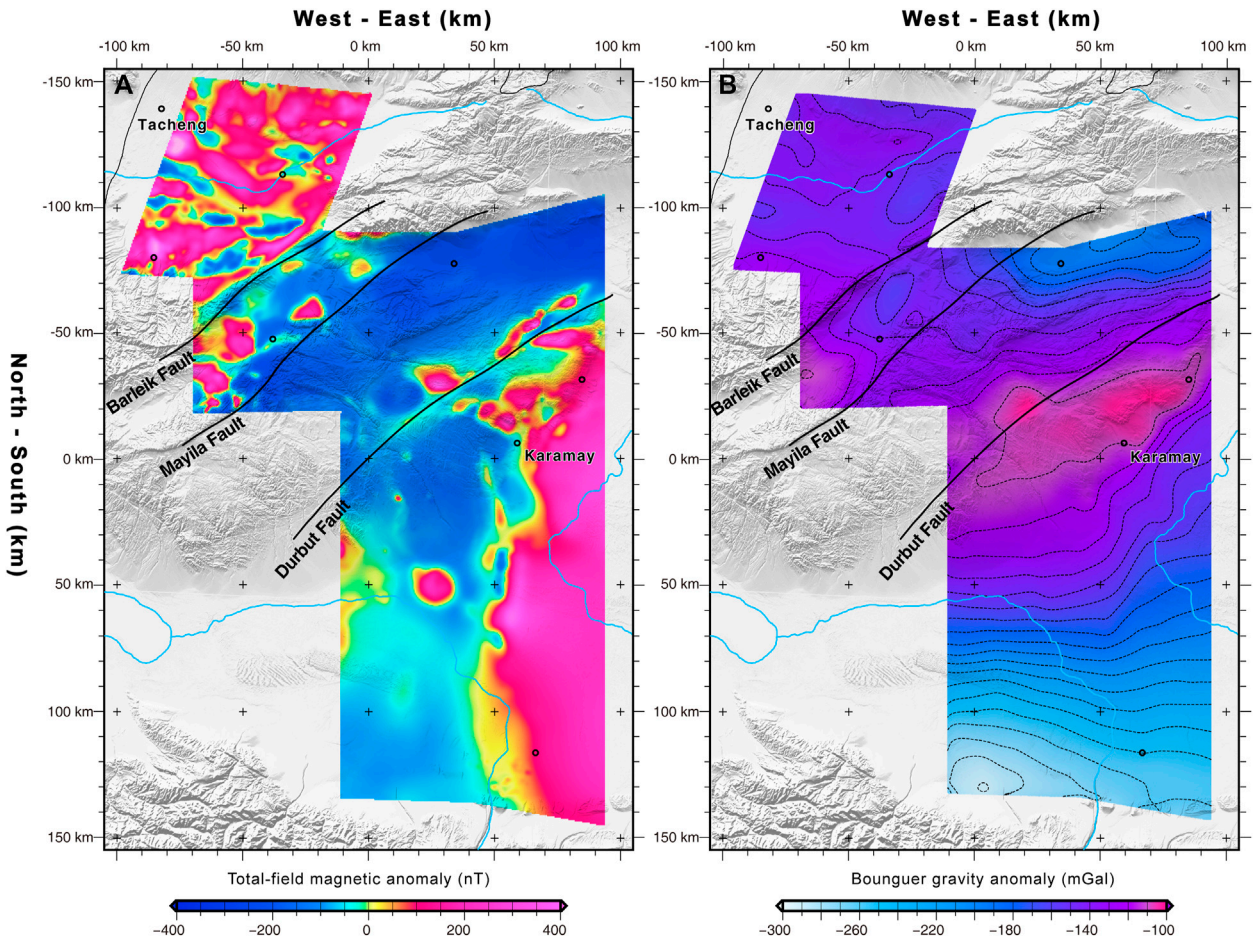

FIGURE 5 | (A) Total-field aeromagnetic anomalies with the reduction to the pole (RTP). The warm red and cool blue shades depict magnetic highs and lows, respectively. **(B)** Aerial Bouguer gravity map with 10-mGal contour intervals. Both maps are overlain on the shaded ETOPO model (www.ngdc.noaa.gov/mgg/global.html).

magnetically, displaying remarkable correlations between the structural and magnetic boundaries. Additionally, to the east of the Darbut fault, the West Junggar Basin is characterized by regional long-wavelength–positive and –negative magnetic anomalies inlaid with local short-wavelength magnetic highs (**Figure 5A**). The basements within the Tacheng Basin and Toli low-topographic valley, expressed by high-frequency positive magnetic anomalies, are more correctly and clearly positioned, as shown in **Figure 4A** than in **Figure 5A**. The regional long-wavelength negative magnetic anomaly dominates the high-topographic mountains between the Mayile and Darbut faults, striking roughly in a NE–SW orientation (**Figure 5A**). Compared with the RTP-corrected magnetic map, the ASA-processed map displays obvious high-frequency signals associated with the magmatism and fault (**Figures 6A**, **7**). In the 3D-shaded ASA map (**Figure 7**), these regional features are further enhanced. Among these noticeable magnetic signals, as we already identified before, this new map is in obvious contrast to the RTP-corrected map. Particularly in the Tacheng Basin and the domains around the Darbut fault, most high-frequency magnetic signals associated with previous magmatism are observed.

The high-precision fundamental data for the understanding of structural components and local geological bodies are provided by airborne Bouguer gravity (Li et al., 2016). The following characteristics can be found in the aerial Bouguer gravity field across the West Junggar. A regional long-wavelength gravity high is located between the Tacheng and West Junggar basins, with a maximum gravity value of +95 mGal, which are all characterized by long-wavelength negative low-value anomalies with a minimum value of −237 mGal (**Figure 4B**). Moreover, in the airborne Bouguer-corrected gravity map (**Figure 5B**), a large-scale long-wavelength gravity high distributes along the Darbut fault with a maximum gravity value of −100.76 mGal, which is surrounded by several local gravity highs to its northwest. Whereas, to its southeast, the West Junggar basin is expressed by the widely distributed negative anomaly low with gravity values ranging from −290.7 mGal to −200 mGal (**Figure 5B**).

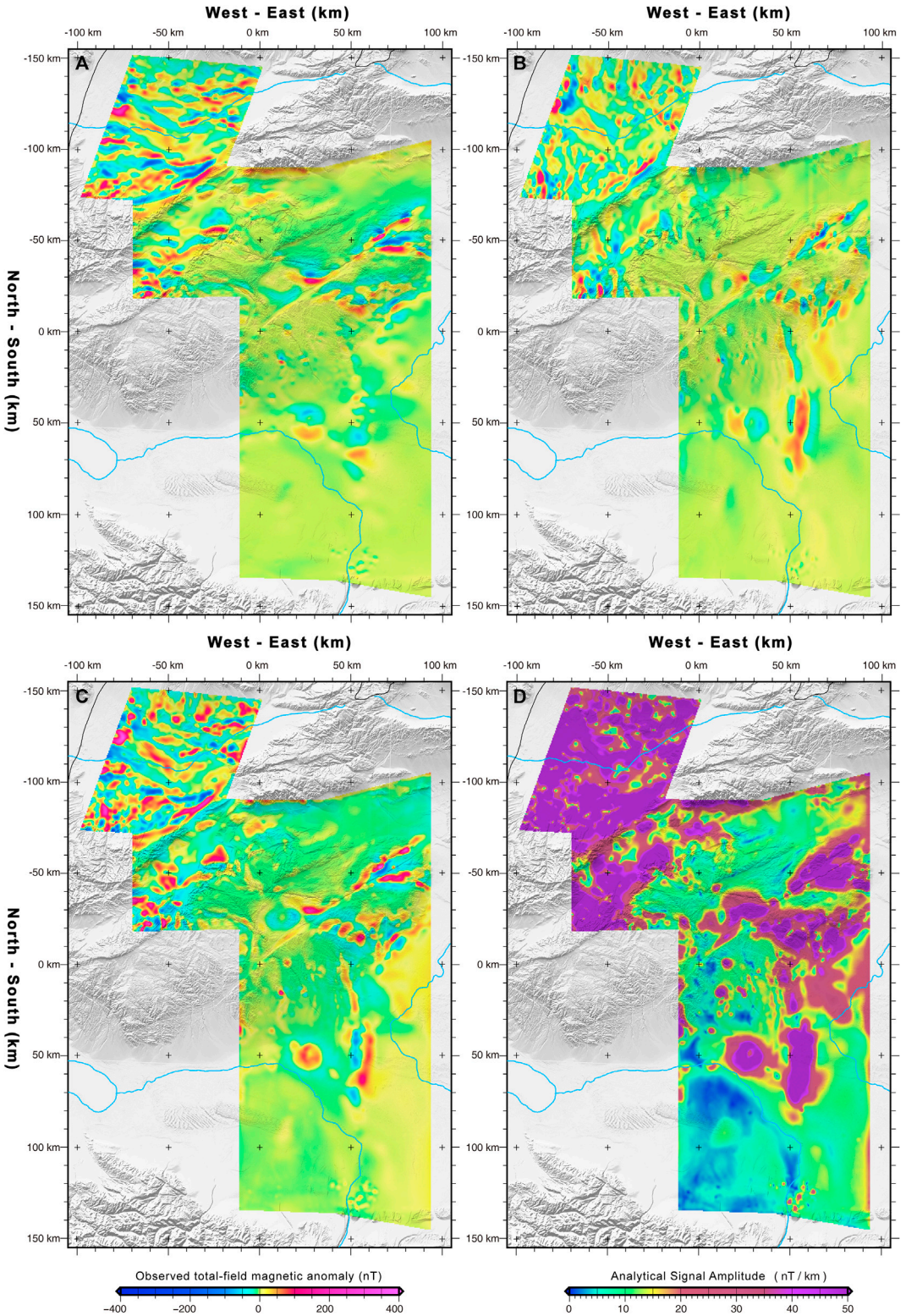

FIGURE 6 | Processed results of the analytic signal of aeromagnetic anomaly. **(A)** Horizontal-X, **(B)** Horizontal-Y, and **(C)** Vertical-Z derivatives are calculated from the total-field aeromagnetic anomaly with the RTP (**Figure 2**). **(D)** Map of analytical signal amplitudes that we processed from total-field magnetic anomalies. All the maps are overlain on the shaded ETOPO model (www.ngdc.noaa.gov/mgg/global.html).

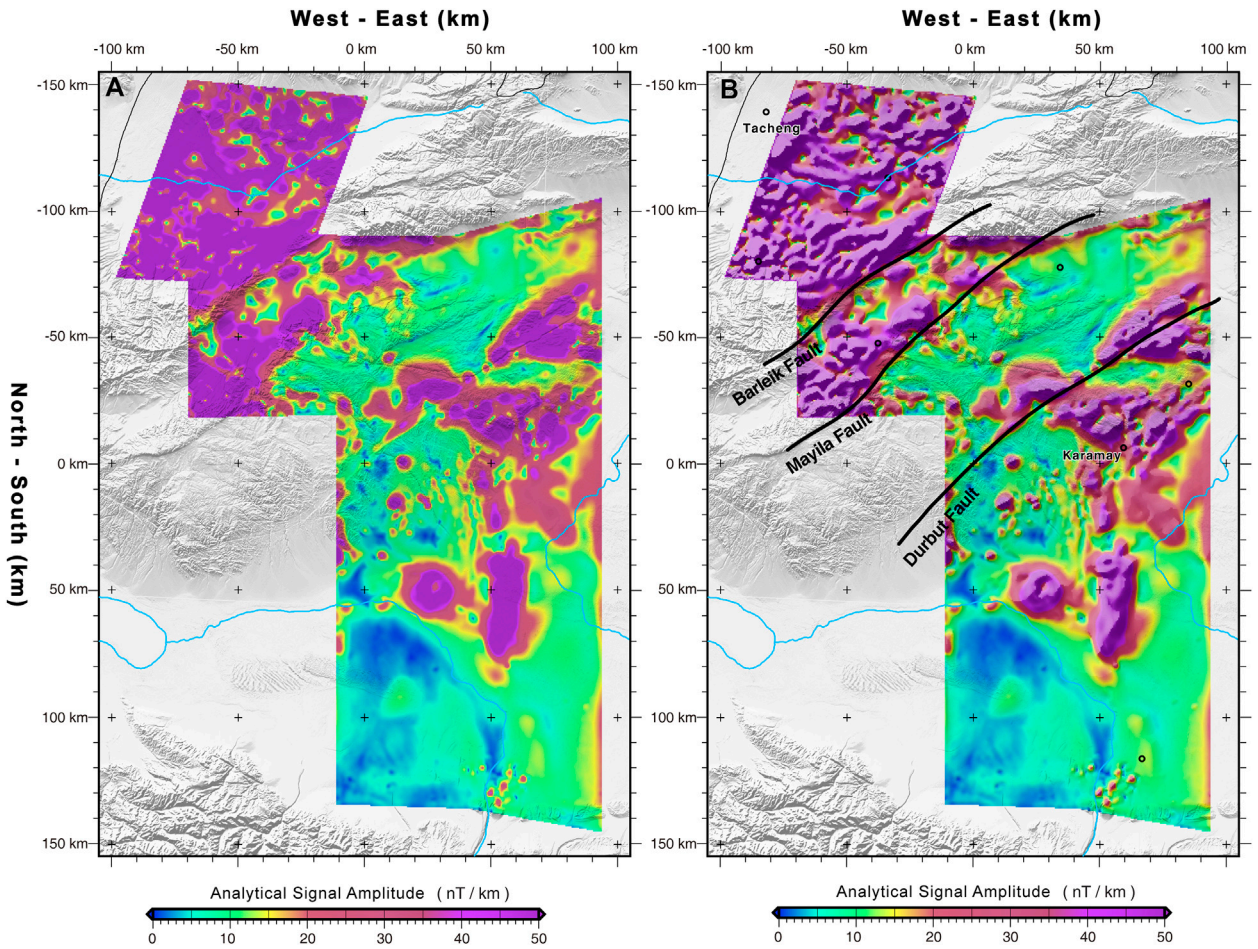

FIGURE 7 | (A) Map of analytical signal amplitudes. **(B)** 3D shaded map of analytical signal amplitudes with key faults.

GEOLOGICAL INTERPRETATION AND DISCUSSION

Based on the increasingly geological, geochemical, and geophysical observations, most recent studies have proposed a subduction-dominated tectonic setting for the West Junggar region (Zhang et al., 2011a, 2011b; Ma et al., 2012; Yin et al., 2013; Xu et al., 2016; Zheng et al., 2017). Especially, in the past five years, high-quality seismological and magnetotelluric sections thoroughly imaged the detailed 2D and 3D geometry of the remnant subducting slab beneath the West Junggar (Xu et al., 2016; Xu et al., 2020; Zhang et al., 2017; Liu et al., 2019). These lithospheric-scale observations provided valid constraints on the origin and geometry of a possible northwestward fossil subducting slab and a well-preserved island arc in the Darbut belt (Xu et al., 2016; Zhang et al., 2017) (**Figure 8**).

Characterized by the low-resistivity conductor, the hidden Karamay–Urho fault separated the Darbut belt and the West Junggar, is naturally interpreted to be a Late-Paleozoic trench that evolved to be a suture in the present-day tectonic context (Xu et al., 2016) (**Figure 8** YY'). Although its geometry could not be traced in the seismic section (**Figure 9** ZZ'), the Carboniferous sedimentary rocks beneath the Darbut belt have been strongly compressed and deformed (Ma et al., 2014), implying that there would exist a northwestward Late-Paleozoic subduction system to its southeast.

Indicated by the structure of shallow flower-shaped faults and sharp offsets of the Moho interface, Xu et al. (2016) proposed that the Karamay–Urho fault could evolve to be a shearing-dominated fault when the subduction failed and subvertically developed to be the oceanic slab remnant. The Darbut zone located between the faults F1 and F2 was interpreted to be a remnant island arc marked by a series of high-conductivity conductors (Xu et al., 2016) (**Figure 8** YY'). Moreover, according to the result of geodynamic modeling (Baitsch-Ghirardello et al., 2014), the domain ranging from Mayile fault to fault F1 was further understood as an intra-arc extension center (i.e., a possible back-arc basin) (Xu et al., 2016). In terms of the lines of the previous evidence, the West Junggar subduction system has finally been proposed, including an accretionary prim, island arc and back-arc basin (**Figure 8** YY').

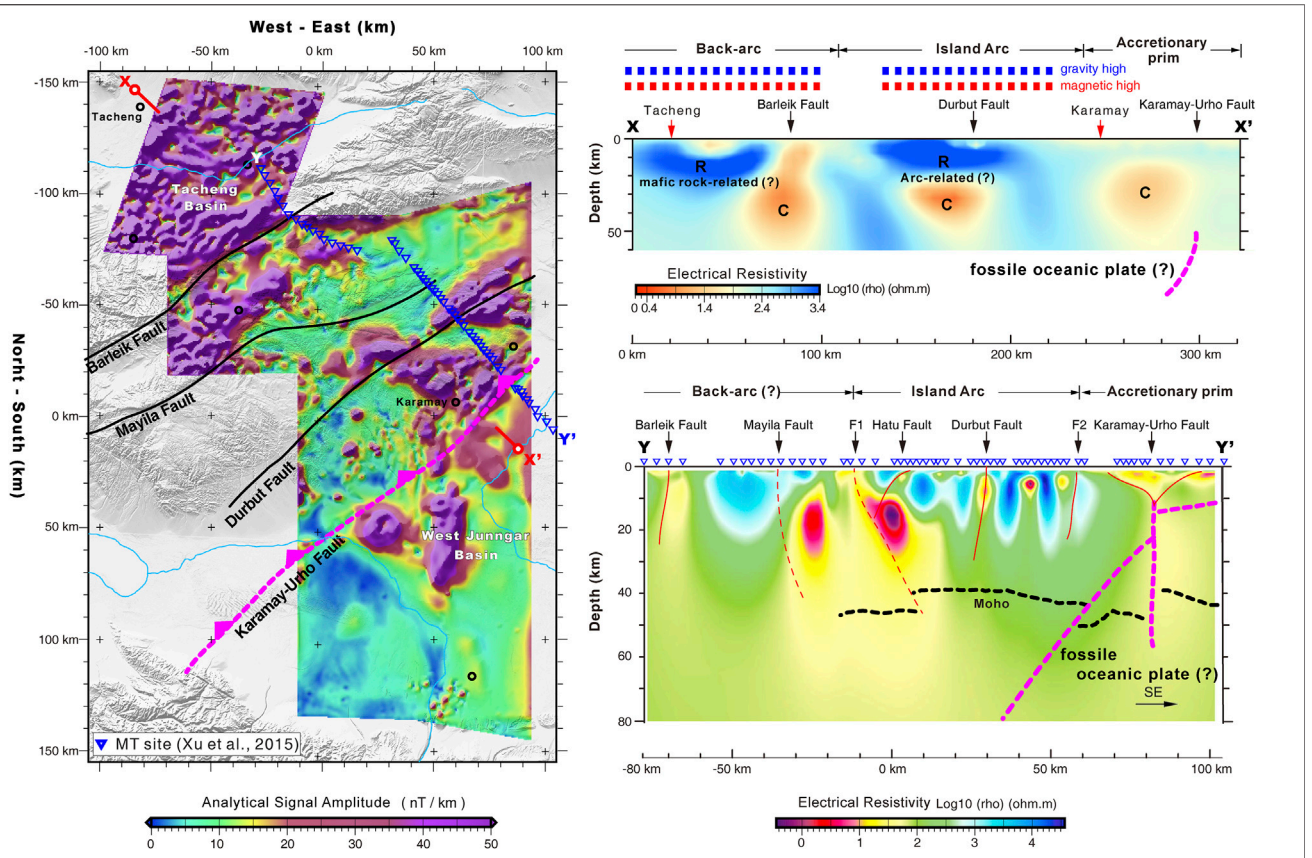

FIGURE 8 | Geological interpretation of airborne magnetic–gravity anomalies, constrained by the resistivity cross section XX' extracted from the 3D MT inversion model of the Xu et al. (2020). Resistivity cross section YY' extracted from the MT profile of Xu et al. (2016) and its tectonic interpretation and corresponding geological model. C, conductor; R, resistor.

In this study, there are two remarkable airborne magnetic–gravity highs across the West Junggar (**Figure 5**; **Figure 8** XX'), which are spatially corresponding to two upper-middle crust-scale horizontal resistors located beneath the Darbut zone and Tacheng Basin (Xu et al., 2020), respectively, thoroughly imaged by the newest three-dimensional (3D) resistivity model (Xu et al., 2020). Particularly, the Tacheng Basin is characterized by high-frequency magnetic and gravity highs (**Figure 5**), well-displayed in the 3D-shaded magnetic ASA map. It is notable that the Tacheng Basin is obviously expressed by a Carboniferous extensional basin with syn-rifting and post-rifting stages, which is clearly revealed by a high-resolution seismic section and strata-dated drill cores (**Figure 9** YY'). This Carboniferous basin is most likely a consequence of mantle upwelling triggered by downgoing oceanic subduction, underplated by mafic–ultramafic melt, and finally floored by mafic-rich, high-magnetic basement (**Figure 8**). Spatially and tectonically, it could be reasonably interpreted as a back-arc basin of the West Junggar subduction system (**Figure 8** XX' and **Figure 9**). Moreover, the magnetic–gravity high across the Darbut belt corresponds to a coupled resistor and conductor beneath the belt (**Figure 8** XX'), which is partially different from the previous MT inversion model (**Figure 8** YY') (Xu et al., 2016). It would be produced in the crust of the island arc under the back-arc tectonic setting of mantle wedge convection (**Figure 9**). Furthermore, focused on the subduction-related structures and volcanic rocks, most geological and geochemical studies suggested that an oceanic ridge–related subduction system may exist during the Carboniferous (Zhang et al., 2011a, 2011b; Tao et al., 2013; Cao et al., 2014; Gao et al., 2014). In summary, a representative double-subduction model has been proposed for the Carboniferous tectonic evolution of West Junggar (Zhang et al., 2011a; Zhang et al., 2011b). Moreover, structural analysis of accretionary complexes between Darbut and Karamay shows that asymmetric folds and thrusts have NW vergence, which means subduction toward SE (Zhang et al., 2011b). These geological–geophysical observations are all valuable constraints for renewing and revising the current widely-accepted geological models. Owing to the limitation of our airborne magnetic–gravity data, it is hard to rule out the possibility of any of the current widely prevalent models. But, following along current systematically integrated geological–geophysical evidence, we tentatively propose a renewed model of Xu et al. (2016, 2020) for the Late Paleozoic West Junggar oceanic-slab subduction-dominated trench-arc-basin system, especially highlighting that the Tacheng Basin could be an important back-arc basin of this system (**Figure 8** YY' and **Figure 9**). In the

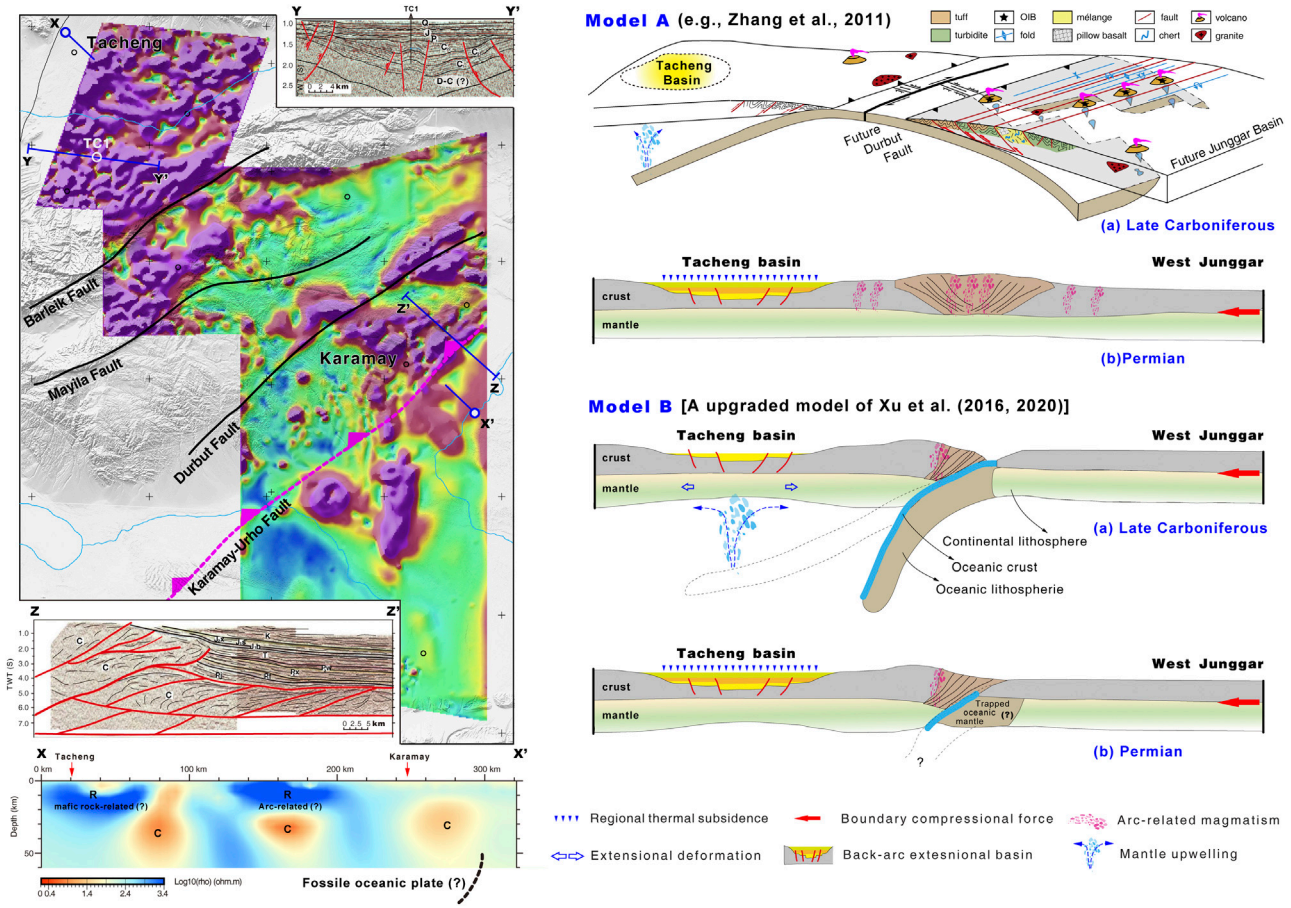

FIGURE 9 | Tectonic model comparisons constrained by geological and geophysical observations. Crust-scale resistivity cross-section XX' extracted from Xu et al. (2020)'s three-dimensional model. Seismic sections YY' and ZZ' are derived from Li et al. (2016) and Ma et al. (2014), respectively. Model A upgraded from Zhang et al. (2011a) and model B (this study) present the tectonic evolution of West Junggar. In model A, constrained by the magnetic–gravity observations, we further interpret the location of the Tacheng Basin. Notably, model B is an upgraded model of Xu et al. (2016, 2020).

future, associated with the geological observations, the systematically integrated geophysical imaging would be urgently required in order to investigate the origin and finely deep structure of such a fossil subduction system.

CONCLUSION

An integrated aerial magnetic–gravity survey consisting of 66,000 survey-line kilometers costing 1.4 million dollars, was deployed in the West Junggar, Xinjiang Province, Northwest China. By systematically processing the surveying data, we obtained a series of high-resolution magnetic and gravity anomaly maps. Integrated with comprehensive geological and geophysical observations, the crust structure of West Junggar has been well imaged in detail. Especially, there is a remarkable Bouguer gravity high located between the Darbut and Karamay–Urho faults, spatially consistent with the remnant oceanic slab detected by the magnetotelluric (MT) investigation of Xu et al. (2016, 2020). Most importantly, the Tacheng Basin characterized by short-wavelength positive magnetic anomalies and series of gravity highs is reasonably interpreted to be a Carboniferous back-arc rifting basin, which is not identified by previous geophysical investigations owing to the limitation of these geophysical approaches. Finally, in terms of newly-processed magnetic–gravity data as well as these geophysical observations across the West Junggar, we further renewed the model of the trench-arc-basin subduction system proposed by previous literature. Some contentious issues on the origin and fine lithosphere structure of the West Junggar subduction system need to be further studied when more integrated geological–geophysical data are available and interpreted in the future (Buslov et al., 2004; Safonova et al., 2011a; Safonova et al., 2011b; Li et al., 2012; Yan et al., 2012; Jian et al., 2013; Di, 2016; Dai et al., 2021).

DATA AVAILABILITY STATEMENT

The original contributions presented in the study are included in the article; further inquiries can be directed to the corresponding author.

AUTHOR CONTRIBUTIONS

XX conceived the study and interpreted the data; QZ compliled the data; XX and QZ wrote the manuscript; WZ and YL checked the manuscript; other co-authors jointly modified the manuscript; YL and WZ oversaw the survey project.

FUNDING

This work is financially supported by the grants from the Key Laboratory of Airborne Geophysics and Remote Sensing Geology Ministry of Natural Resources (No. 2020YFL13), Chinese Postdoctoral Science Foundation (No. 2019M652062), the National Science Foundation of China (41902202), and the Geological Survey Project of China (No. DD20211396 and 12120115039301).

ACKNOWLEDGMENTS

We greatly thank all the coworkers for their efforts on the field work of the survey project, including Bing Li, Zhibo Wang, Xiujuan Liang, Xue Yang, Rui Li, and Chenyang Wang. We appreciate the sincere discussion with Prof. Yigui Han, Northwest University, and Prof. Yixian Xu, Zhejiang University.

REFERENCES

Agarwal, B. N. P., and Shaw, R. K. (1996). Comment on 'An Analytic Signal Approach to the Interpretation of Total Field Magnetic Anomalies' by Shuang Qin1. *Geophys. Prospect* 44 (5), 911–914. doi:10.1111/j.1365-2478.1996.tb00180.x

Allen, M. B., aengör, A. M. C., and Natal'In, B. A. (1995). Junggar, Turfan and Alakol Basins as Late Permian to ?Early Triassic Extensional Structures in a Sinistral Shear Zone in the Altaid Orogenic Collage, Central Asia. *J. Geol. Soc.* 152 (2), 327–338. doi:10.1144/gsjgs.152.2.0327

Arkani-Hamed, J. (1988). Differential Reduction-to-the-pole of Regional Magnetic Anomalies. *Geophysics* 53 (12), 1592–1600. doi:10.1190/1.1442441

Baitsch-Ghirardello, B., Stracke, A., Connolly, J. A. D., Nikolaeva, K. M., and Gerya, T. V. (2014). Lead Transport in Intra-oceanic Subduction Zones: 2D Geochemical-Thermo-Mechanical Modeling of Isotopic Signatures. *Lithos* 208-209, 265–280. doi:10.1016/j.lithos.2014.09.006

Buckman, S., and Aitchison, J. C. (2004). Tectonic Evolution of Palaeozoic Terranes in West Junggar, Xinjiang, NW China. *Geol. Soc. Lond. Spec. Publications* 226 (1), 101–129. doi:10.1144/GSL.SP.2004.226.01.06

Buslov, M. M., Fujiwara, Y., Iwata, K., and Semakov, N. N. (2004). Late Paleozoic-Early Mesozoic Geodynamics of Central Asia. *Gondwana Res.* 7 (3), 791–808. doi:10.1016/S1342-937X(05)71064-9

Cao, M., Qin, K., Li, G., Jin, L., Evans, N. J., and Yang, X. (2014). Baogutu: An Example of Reduced Porphyry Cu deposit in Western Junggar. *Ore Geology. Rev.* 56, 159–180. doi:10.1016/j.oregeorev.2013.08.014

Chen, B., and Arakawa, Y. (2005). Elemental and Nd-Sr Isotopic Geochemistry of Granitoids from the West Junggar Foldbelt (NW China), with Implications for Phanerozoic continental Growth. *Geochimica et Cosmochimica Acta.* 69 (5), 1307–1320. doi:10.1016/j.gca.2004.09.019

Chen, S., Pe-Piper, G., Piper, D. J. W., and Guo, Z. (2014). Ophiolitic Mélanges in Crustal-Scale Fault Zones: Implications for the Late Palaeozoic Tectonic Evolution in West Junggar, China. *Tectonics* 33 (12), 2419–2443. doi:10.1002/2013TC003488

Choulet, F., Faure, M., Cluzel, D., Chen, Y., Lin, W., and Wang, B. (2012). From Oblique Accretion to Transpression in the Evolution of the Altaid Collage: New Insights from West Junggar, Northwestern China. *Gondwana Res.* 21 (2), 530–547. doi:10.1016/j.gr.2011.07.015

Coleman, R. G. (1989). Continental Growth of Northwest China. *Tectonics* 8 (3), 621–635. doi:10.1029/TC008i003p00621

Dai, X., Korn, D., and Song, H. (2021). Morphological Selectivity of the Permian-Triassic Ammonoid Mass Extinction. *Geology* 49, 1112–1116. doi:10.1130/G48788.1

Di, L. (2016). *Carboniferous Tectonic Framework and Sedimentary Filling Evolution in the Junggar Basin and Adjacent Area, NW China*. Beijing: China University of Geosciences. (in Chinese with English abstract).

Feng, Y., Coleman, R. G., Tilton, G., and Xiao, X. (1989). Tectonic Evolution of the West Junggar Region, Xinjiang, China. *Tectonics* 8 (4), 729–752. doi:10.1029/TC008i004p00729

Gao, R., Xiao, L., Pirajno, F., Wang, G.-c., He, X.-x., Yang, G., et al. (2014). Carboniferous-Permian Extensive Magmatism in the West Junggar, Xinjiang, Northwestern China: its Geochemistry, Geochronology, and Petrogenesis. *Lithos* 204, 125–143. doi:10.1016/j.lithos.2014.05.028

Geng, H., Sun, M., Yuan, C., Xiao, W., Xian, W., Zhao, G., et al. (2009). Geochemical, Sr-Nd and Zircon U-Pb-Hf Isotopic Studies of Late Carboniferous Magmatism in the West Junggar, Xinjiang: Implications for ridge Subduction. *Chem. Geology.* 266 (3), 364–389. doi:10.1016/j.chemgeo.2009.07.001

Han, Y., and Zhao, G. (2018). Final Amalgamation of the Tianshan and Junggar Orogenic Collage in the Southwestern Central Asian Orogenic Belt: Constraints on the Closure of the Paleo-Asian Ocean. *Earth-Science Rev.* 186, 129–152. doi:10.1016/j.earscirev.2017.09.012

He, G. Q., Jianbo, L., Yueqian, Z., and Xin, X. (2007). Keramay Ophiolitic Mélange Formed during Early Paleozoic in Western Junggar basin. *Acta Petrologica Sinica* 23 (7), 1573–1576 [in Chinese with English abstract].

Jahn, B.-m., Capdevila, R., Liu, D., Vernon, A., and Badarch, G. (2004). Sources of Phanerozoic Granitoids in the Transect Bayanhongor-Ulaan Baatar, Mongolia: Geochemical and Nd Isotopic Evidence, and Implications for Phanerozoic Crustal Growth. *J. Asian Earth Sci.* 23 (5), 629–653. doi:10.1016/S1367-9120(03)00125-1

Jahn, B.-m., Wu, F., and Chen, B. (2000). Granitoids of the Central Asian Orogenic Belt and continental Growth in the Phanerozoic. *Earth Environ. Sci. Trans. R. Soc. Edinb.* 91 (1-2), 181–193. doi:10.1017/S0263593300007367

Jian, P., Kröner, A., Jahn, B.-m., Liu, D., Zhang, W., Shi, Y., et al. (2013). Zircon Ages of Metamorphic and Magmatic Rocks within Peridotite-Bearing Mélanges: Crucial Time Constraints on Early Carboniferous Extensional Tectonics in the Chinese Tianshan. *Lithos* 172-173, 243–266. doi:10.1016/j.lithos.2013.04.018

Kröner, A., Hegner, E., Lehmann, B., Heinhorst, J., Wingate, M. T. D., Liu, D. Y., et al. (2008). Palaeozoic Arc Magmatism in the Central Asian Orogenic Belt of Kazakhstan: SHRIMP Zircon Ages and Whole-Rock Nd Isotopic Systematics. *J. Asian Earth Sci.* 32 (2), 118–130. doi:10.1016/j.jseaes.2007.10.013

Kröner, A., Windley, B. F., Badarch, G., Tomurtogoo, O., Hegner, E., Jahn, B. M., et al. (2007). Accretionary Growth and Crust Formation in the Central Asian Orogenic Belt and Comparison with the Arabian-Nubian Shield. *Memoir Geol. Soc. America* 200, 181–209. doi:10.1130/2007.1200(11)

Li, C.-F., Wang, J., Zhou, Z., Geng, J., Chen, B., Yang, F., et al. (2012). 3D Geophysical Characterization of the Sulu-Dabie Orogen and its Environs. *Phys. Earth Planet. Interiors* 192-193, 35–53. doi:10.1016/j.pepi.2012.01.003

Li, D., He, D., Qi, X., and Zhang, N. (2015b). How Was the Carboniferous Balkhash-West Junggar Remnant Ocean Filled and Closed? Insights from the Well Tacan-1 Strata in the Tacheng Basin, NW China. *Gondwana Res.* 27 (1), 342–362. doi:10.1016/j.gr.2013.10.003

Li, D., He, D., Santosh, M., Ma, D., and Tang, J. (2015a). Tectonic Framework of the Northern Junggar Basin Part I: The Eastern Luliang Uplift and its Link with the East Junggar Terrane. *Gondwana Res.* 27 (3), 1089–1109. doi:10.1016/j.gr.2014.08.015

Li, D., He, D., Yang, Y., and Lian, Y. (2014). Petrogenesis of Mid-carboniferous Volcanics and Granitic Intrusions from Western Junggar Basin Boreholes: Geodynamic Implications for the Central Asian Orogenic Belt in Northwest

China. *Int. Geology. Rev.* 56 (13), 1668–1690. doi:10.1080/00206814.2014.958766

Li, W., Liu, Y., Li, B., and Luo, F. (2016). Hydrocarbon Exploration in the South Yellow Sea Based on Airborne Gravity, China. *J. Earth Sci.* 27 (4), 686–698. doi:10.1007/s12583-015-0607-y

Li, X. (2006). Understanding 3D Analytic Signal Amplitude. *Geophysics* 71 (2), L13–L16. doi:10.1190/1.2184367

Liu, Y., Wang, X., Wu, K., Chen, S., Shi, Z., and Yao, W. (2019). Late Carboniferous Seismic and Volcanic Record in the Northwestern Margin of the Junggar Basin: Implication for the Tectonic Setting of the West Junggar. *Gondwana Res.* 71, 49–75. doi:10.1016/j.gr.2019.01.013

Ma, C., Xiao, W., Windley, B. F., Zhao, G., Han, C., Zhang, J. e., et al. (2012). Tracing a Subducted ridge-transform System in a Late Carboniferous Accretionary Prism of the Southern Altaids: Orthogonal Sanukitoid Dyke Swarms in Western Junggar, NW China. *Lithos* 140-141, 152–165. doi:10.1016/j.lithos.2012.02.005

Ma, D. (2014). The Structural Geometric and Kinematic Feactures of Wuerhe-Xiazijie Thrust Belt at the Northwestern Margin of Junggar Basin. Master Thesis. Beijing: China University of Geosciences.

Nabighian, M. N. (1984). Toward a Three-dimensional Automatic Interpretation of Potential Field Data via Generalized Hilbert Transforms: Fundamental Relations. *Geophysics* 49 (6), 780–786. doi:10.1190/1.1441706

Ofoegbu, C. O., and Mohan, N. L. (1990). Interpretation of Aeromagnetic Anomalies over Part of southeastern Nigeria Using Three-Dimensional Hilbert Transformation. *Pageoph* 134 (1), 13–29. doi:10.1007/BF00878077

Roest, W. R., Verhoef, J., and Pilkington, M. (1992). Magnetic Interpretation Using the 3-D Analytic Signal. *Geophysics* 57 (1), 116–125. doi:10.1190/1.1443174

Safonova, I., Seltmann, R., Kröner, A., Gladkochub, D., Schulmann, K., Xiao, W., et al. (2011a). A New Concept of continental Construction in the Central Asian Orogenic Belt. *Episodes* 34 (3), 186–196. doi:10.18814/epiiugs/2011/v34i3/005

Safonova, I. Y., Buslov, M. M., Simonov, V. A., Izokh, A. E., Komiya, T., Kurganskaya, E. V., et al. (2011b). Geochemistry, Petrogenesis and Geodynamic Origin of Basalts from the Katun' Accretionary Complex of Gorny Altai (Southwestern Siberia). *Russ. Geology. Geophys.* 52 (4), 421–442. doi:10.1016/j.rgg.2011.03.005

Salem, A., Ravat, D., Gamey, T. J., and Ushijima, K. (2002). Analytic Signal Approach and its Applicability in Environmental Magnetic Investigations. *J. Appl. Geophys.* 49 (4), 231–244. doi:10.1016/S0926-9851(02)00125-8

Sandwell, D., Garcia, E., Soofi, K., Wessel, P., Chandler, M., and Smith, W. H. F. (2013). Toward 1-mGal Accuracy in Global marine Gravity from CryoSat-2, Envisat, and Jason-1. *The Leading Edge* 32 (8), 892–899. doi:10.1190/tle32080892.1

Sandwell, D. T., Müller, R. D., Smith, W. H. F., Garcia, E., and Francis, R. (2014). New Global marine Gravity Model from CryoSat-2 and Jason-1 Reveals Buried Tectonic Structure. *Science* 346 (6205), 65–67. doi:10.1126/science.1258213

Şengör, A. M. C., Natal'in, B. A., and Natal'in, V. S. (1993). Evolution of the Altaid Tectonic Collage and Palaeozoic Crustal Growth in Eurasia. *Nature* 364 (6435), 299–307. doi:10.1038/364299a0

Su, Y. P., Tang, H. F., Hou, G. S., and Liu, C. Q. (2006). Geochemistry of Aluminous A-type Granites along Darabut Tectonic belt in West Junggar, Xinjiang. *Geochimica* 35 (1), 55–67 [in Chinese with English abstract].

Tao, H., Wang, Q., Yang, X., and Jiang, L. (2013). Provenance and Tectonic Setting of Late Carboniferous Clastic Rocks in West Junggar, Xinjiang, China: A Case from the Hala-Alat Mountains. *J. Asian Earth Sci.* 64, 210–222. doi:10.1016/j.jseaes.2012.12.019

Tong, J., Zhang, X., Zhang, W., and Xiong, S. (2018). Marine Strata Morphology of the South Yellow Sea Based on High-Resolution Aeromagnetic and Airborne Gravity Data. *Mar. Pet. Geology.* 96, 429–440. doi:10.1016/j.marpetgeo.2018.06.018

Wessel, P., Smith, W. H. F., Scharroo, R., Luis, J., and Wobbe, F. (2013). Generic Mapping Tools: Improved Version Released. *Eos Trans. AGU* 94 (45), 409–410. doi:10.1002/2013EO450001

Windley, B. F., Alexeiev, D., Xiao, W., Kröner, A., and Badarch, G. (2007). Tectonic Models for Accretion of the Central Asian Orogenic Belt. *J. Geol. Soc.* 164 (1), 31–47. doi:10.1144/0016-76492006-022

Wu, S., Huang, R., Xu, Y., Yang, Y., Jiang, X., and Zhu, L. (2018). Seismological Evidence for a Remnant Oceanic Slab in the Western Junggar, Northwest China. *J. Geophys. Res. Solid Earth* 123 (5), 4157–4170. doi:10.1029/2017JB015332

Xiao, W., Han, C., Yuan, C., Sun, M., Lin, S., Chen, H., et al. (2008). Middle Cambrian to Permian Subduction-Related Accretionary Orogenesis of Northern Xinjiang, NW China: Implications for the Tectonic Evolution of central Asia. *J. Asian Earth Sci.* 32 (2), 102–117. doi:10.1016/j.jseaes.2007.10.008

Xiao, W., and Kusky, T. (2009). Geodynamic Processes and Metallogenesis of the Central Asian and Related Orogenic Belts: Introduction. *Gondwana Res.* 16 (2), 167–169. doi:10.1016/j.gr.2009.05.001

Xiao, W., Windley, B. F., Sun, S., Li, J., Huang, B., Han, C., et al. (2015). A Tale of Amalgamation of Three Permo-Triassic Collage Systems in Central Asia: Oroclines, Sutures, and Terminal Accretion. *Annu. Rev. Earth Planet. Sci.* 43 (1), 477–507. doi:10.1146/annurev-earth-060614-105254

Xiong, S., Yang, H., Ding, Y., Li, Z., and Li, W. (2016). Distribution of Igneous Rocks in China Revealed by Aeromagnetic Data. *J. Asian Earth Sci.* 129, 231–242. doi:10.1016/j.jseaes.2016.08.016

XJBGMR (Bureau of Geology and Mineral Resources of Xinjiang Province) (1993). *m Regional Geology of the Xinjiang Province*. Beijing: Geological Publishing House. (in Chinese with English abstract).

Xu, S. F., Chen, C., Du, J. S., Sun, S. D., and Hu, Z. W. (2015). Characteristics and Tectonic Implications of Lithospheric Density Structures beneath Western Junggar and its Surroundings. *Earth Science (Journal China Univ. Geosciences).* 40 (9), 1556–1565. doi:10.3799/dqkx.2015.140

Xu, X., He, G., Li, H., Ding, T., Liu, X., and Mei, S. (2006). Basic Characteristics of the Karamay Ophiolitic Mélange, Xinjiang, and its Zircon SHRIMP Dating. *Geology. China* 33 (3), 470–475 [in Chinese with English abstract].

Xu, Y. X., Yang, B., Zhang, A. Q., Wu, S. C., Zhu, L., Yang, Y. J., et al. (2020). Magnetotelluric Imaging of a Fossil Oceanic Plate in Northwestern Xinjiang, China. *Geology* 48 (4), 385–389. doi:10.1130/G47053.1

Xu, Y., Yang, B., Zhang, S., Liu, Y., Zhu, L., Huang, R., et al. (2016). Magnetotelluric Imaging of a Fossil Paleozoic Intraoceanic Subduction Zone in Western Junggar, NW China. *J. Geophys. Res. Solid Earth* 121 (6), 4103–4117. doi:10.1002/2015JB012394

Yan, C., Chen, C., Cao, X., Zhang, W., Chen, J., Li, S., et al. (2012). The Discovery of the "Pamir-type" Iron Deposits in Taxkorgan Area of Xinjiang and its Geological Significance. *Geol. Bull. China* 31 (4), 549–557 [in Chinese with English abstract].

Yang, G., Li, Y., Santosh, M., Yang, B., Yan, J., Zhang, B., et al. (2012). Geochronology and Geochemistry of Basaltic Rocks from the Sartuohai Ophiolitic Mélange, NW China: Implications for a Devonian Mantle Plume within the Junggar Ocean. *J. Asian Earth Sci.* 59, 141–155. doi:10.1016/j.jseaes.2012.07.020

Yang, G., Li, Y., Santosh, M., Yang, B., Zhang, B., and Tong, L. (2013). Geochronology and Geochemistry of Basalts from the Karamay Ophiolitic Melange in West Junggar (NW China): Implications for Devonian-Carboniferous Intra-oceanic Accretionary Tectonics of the Southern Altaids. *Geol. Soc. America Bull.* 125 (3-4), 401–419. doi:10.1130/b30650.1

Yang, G., Li, Y., Xiao, W., and Tong, L. (2015a). OIB-type Rocks within West Junggar Ophiolitic Mélanges: Evidence for the Accretion of Seamounts. *Earth-Science Rev.* 150, 477–496. doi:10.1016/j.earscirev.2015.09.002

Yang, Y.-T., Song, C.-C., and He, S. (2015b). Jurassic Tectonostratigraphic Evolution of the Junggar basin, NW China: A Record of Mesozoic Intraplate Deformation in Central Asia. *Tectonics* 34 (1), 86–115. doi:10.1002/2014tc003640

Yin, J., Long, X., Yuan, C., Sun, M., Zhao, G., and Geng, H. (2013). A Late Carboniferous-Early Permian Slab Window in the West Junggar of NW China: Geochronological and Geochemical Evidence from Mafic to Intermediate Dikes. *Lithos* 175-176, 146–162. doi:10.1016/j.lithos.2013.04.005

Zhang, C., and Huang, X. (1992). The Ages and Tectonic Settings of Ophiolites in West Junggar, Xinjiang. *Geol. Rev.* 38 (6), 509–524.

Zhang, J. e., Chen, Y., Xiao, W., Wakabayashi, J., Windley, B. F., and Yin, J. (2021). Sub-parallel ridge-trench interaction and an alternative model for the Silurian-Devonian archipelago in Western Junggar and North-Central Tianshan in NW China. *Earth-Science Reviews* 217, 103648. doi:10.1016/j.earscirev.2021.103648

Zhang, J. e., Xiao, W., Han, C., Ao, S., Yuan, C., Sun, M., et al. (2011a). Kinematics and Age Constraints of Deformation in a Late Carboniferous Accretionary

Complex in Western Junggar, NW China. *Gondwana Res.* 19 (4), 958–974. doi:10.1016/j.gr.2010.10.003

Zhang, J. e., Xiao, W., Han, C., Mao, Q., Ao, S., Guo, Q., et al. (2011b). A Devonian to Carboniferous Intra-oceanic Subduction System in Western Junggar, NW China. *Lithos* 125 (1), 592–606. doi:10.1016/j.lithos.2011.03.013

Zhang, J. E., Xiao, W., Luo, J., Chen, Y., Windley, B. F., Song, D., et al. (2018). Collision of the Tacheng Block with the Mayile-Barleik-Tangbale Accretionary Complex in Western Junggar, NW China: Implication for Early-Middle Paleozoic Architecture of the Western Altaids. *J. Asian Earth Sci.* 159, 259–278. doi:10.1016/j.jseaes.2017.03.023

Zhang, S., Xu, Y., Jiang, L., Yang, B., Liu, Y., Griffin, W. L., et al. (2017). Electrical Structures in the Northwest Margin of the Junggar basin: Implications for its Late Paleozoic Geodynamics. *Tectonophysics* 717, 473–483. doi:10.1016/j.tecto.2017.08.031

Zheng, G., Ma, X., Guo, Z., Hilton, D. R., Xu, W., Liang, S., et al. (2017). Gas Geochemistry and Methane Emission from Dushanzi Mud Volcanoes in the Southern Junggar Basin, NW China. *J. Asian Earth Sci.* 149, 184–190. doi:10.1016/j.jseaes.2017.08.023

Conflict of Interest: The authors declare that the research was conducted in the absence of any commercial or financial relationships that could be construed as a potential conflict of interest.